Isotropic and Anisotropic Flux Pinning Induced by Heavy-Ion Irradiation

Nicholas M. Strickland, Stuart C. Wimbush, *Senior Member, IEEE*, Arya A. Soman, Patrick Kluth, Christian Notthoff, Ruth Knibbe, Ming Li, and Martin W. Rupich

***Abstract*—Ion irradiation of REBCO films and coated conductors, in which the ions pass completely through the REBCO film, produces damage tracks which form near-ideal flux-pinning defects. The radius and aspect ratio of the tracks depends on the mass and energy of the incident ions. We have investigated the effect of Ag ion irradiation, at different incident energies and incidence angles, on REBCO production-quality coated conductors from American Superconductor Corp. Transmission electron microscopy and in-field transport critical current anisotropy analysis indicates that the ion-energy threshold for the formation of elongated tracks is around 50 MeV. At this energy tracks are not readily identifiable in low-resolution TEM, and enhancement of critical current is nearly isotropic. For a higher ion energy of 100 MeV, on the other hand, clear elongated (but still not fully continuous) tracks are visible in TEM, and the critical current is anisotropic with strong enhancement occurring when the applied field is parallel to the ion incidence angle. We particularly analyze the case of 60° inclined irradiation. This produces a clear peak in the field-angle dependence of critical current for 100 MeV irradiation, but only an incipient peak for 50 MeV irradiation. The incipient peak can be identified by curve fitting using a minimal number of maximum-entropy functional components.**

***Index Terms*—Coated conductors, critical current anisotropy, ion irradiation, REBCO.**

I. Introduction

HIGH temperature superconducting (HTS) wires based on $REBa_2Cu_3O_7$ (REBCO, where RE = rare-earth elements or yttrium) thick films on metal foil substrates can readily be modified to introduce flux-pinning defects to improve critical current (I_c) performance in the presence of a magnetic field. The interaction between the vortex lattice and multiple populations of pinning defects is extremely complex, and a deeper understanding of this is critical to the goal of engineering an optimized critical current anisotropy [1], [2].

Secondary-phase or dopant inclusions and growth defects with suitable dimensions to provide flux pinning can be engineered during deposition or growth of the film [3]–[5]. Huge gains have been made in improving flux pinning through these methods, which can often be implemented with negligible extra cost other than development time. A disadvantage of this approach is that it is generally not possible to change the prevalence or dimensions of one type of defect without having significant knock-on effects on other defect populations or on the YBCO matrix itself. I_c enhancements are often attributed to one modification when several other factors may also be important.

Ion beam irradiation can form a useful complement to the modifications produced in production [6]–[14]. As usual, "irradiation" implies that the ions pass completely through the REBCO film and it is the amorphized damage tracks left by their interaction with ions in the film that serve as additional flux pinning centers. These tracks typically have radii up to a few nanometers, making them a close match to the superconducting coherence length and therefore excellent pinning centers in REBCO. The process of irradiation also nominally does not disrupt the existing defect landscape, so it is nearly a perfectly additive process. In contrast, the flux pinning that arises from the new landscape, manifested in the critical current, is not additive in a simple way – for example splayed irradiation columnar defects can combine to produce a single peak that does not correspond to an additive combination of the two individual peaks alone [7], [10]. Thus, with ion irradiation we can create pinning landscapes with controlled defect densities and dimensions, and we can begin to quantify the structure-property relationship to understand how defects combine to produce a given critical current anisotropy.

II. Experimental Methods

The starting material for this study was a long-length coated conductor taken from the American Superconductor Corp. production line [15]. This tape was finished with a thinner-than-usual silver cap layer of only 1 μm thickness to minimize the impact on the energy of the incident ion beam. No further plating or lamination layers were added. The HTS layer, deposited by metal-organic deposition, was approximately 1.4 μm thick and

Manuscript received September 23, 2021; revised November 22, 2021; accepted December 25, 2021. Date of publication January 13, 2022; date of current version February 4, 2022. This work was supported in part by the Royal Society of New Zealand under Marsden Fund under Grant VUW1805. *(Corresponding author: Nicholas M. Strickland.)*

Nicholas M. Strickland, Stuart C. Wimbush, and Arya A. Soman are with the Robinson Research Institute, Victoria University of Wellington, Lower Hutt 5010, New Zealand (e-mail: nick.strickland@vuw.ac.nz; stuart.wimbush@vuw.ac.nz; arya.ambadiyilsoman@vuw.ac.nz).

Patrick Kluth and Christian Notthoff are with the Research School of Physics, Australian National University, Canberra, ACT 2601, Australia (e-mail: patrick.kluth@anu.edu.au; christian.notthoff@anu.edu.au).

Ruth Knibbe and Ming Li are with the School of Mechanical and Mining Engineering, The University of Queensland, Brisbane, QLD 4072, Australia (e-mail: ruth.knibbe@uq.edu.au; m.li7@uq.edu.au).

Martin W. Rupich is with American Superconductor Corporation, Ayer, MA 01432 USA (e-mail: marty.rupich@amsc.com).

Color versions of one or more figures in this article are available at https://doi.org/10.1109/TASC.2022.3142715.

Digital Object Identifier 10.1109/TASC.2022.3142715

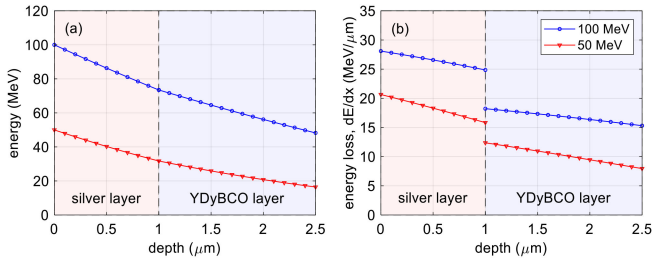

Fig. 1. The reduction in (a) energy and (b) the energy loss of Ag ions passing through a Ag – (Y,Dy)BCO film stack, calculated for incident ion energies of 100 MeV and 50 MeV.

had the nominal composition $YBa_2Cu_3O_7 + 0.25\ Dy_2O_3$. The excess rare-earth oxide forms incoherent nanoparticles within the REBCO matrix and it is understood that the Y and Dy substitute for one another between the matrix and the nanoparticles.

Short samples cut from the long tape were patterned to form a 0.5 mm $\times$ 5 mm current bridge using photolithography and wet chemical etching to match the ion beam irradiation area and to limit the current required for characterization.

Irradiation with 50 MeV or 100 MeV Ag ions to a fluence of 2×10^{11} ions/cm^2 was undertaken at the Heavy Ion Accelerator Facility at the Australian National University.

Sample cross sections were prepared with a FEI Scios focused ion beam system and images were taken with a Hitachi HF 5000 transmission electron microscope (TEM).

The transport critical current (I_c) of each sample was characterized over a range of temperatures, applied magnetic fields and field angles on a SuperCurrent Measurement System [16]. The magnetic field was applied in the maximum Lorentz force configuration, i.e., rotated in the plane perpendicular to the transport current and the field angle θ is here defined to be relative to the tape normal. The electric-field criterion for determining I_c was taken as 1 μV/cm.

III. Ion Energy Profiles

The energy E_i of the ions decreases as it passes through first the silver cap layer and secondly the REBCO film itself. The nature of the defects generated depends on the rate of energy loss $S = dE_i/dx$ which itself is a function of E_i and the target material. The form of $S(E_i)$ for different ions and target materials can be calculated by Monte-Carlo simulations and is available from the SRIM software package [17]. From this form it is straightforward to determine both the energy and energy loss as functions of depth through the composite sample. This is shown in Fig. 1 for 100 MeV and 50 MeV Ag ions incident on the sample consisting of a 1 μm silver layer on top of a 1.4 μm REBCO layer. Because of the silver layer, the ion energy incident on the REBCO layer is significantly lower than the initial energy and reduces further as it passes through. The energy in the REBCO film ranges from about 73 MeV to 50 MeV and from 32 MeV to 17 MeV for incident energies of 100 MeV and 50 MeV, respectively. Similarly the energy loss reduces from 15 MeV/μm to 18 MeV/μm and from 8 MeV/μm to 12 MeV/μm for 100 MeV and 50 MeV starting ions respectively.

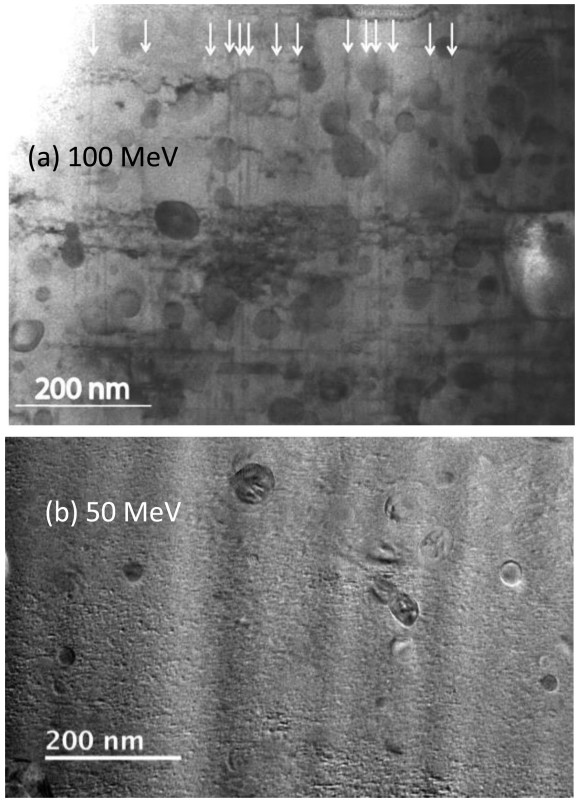

Fig. 2. Low-resolution TEM micrograph of part of the REBCO film following irradiation with (a) 100 MeV and (b) 50 MeV Ag ions. The ion beam was incident from the top of the image and for 100 MeV produced the discontinuous columnar tracks indicated by arrows. Irradiation-induced defects have not yet been identified in the 50 MeV sample. $(Y,Dy)_2O_3$ nanoparticles and *ab*-planar defects also evident are typical of the pristine non-irradiated samples.

These energy loss ranges suggest that 100 MeV ions should produce elongated discontinuous columnar tracks, while 50 MeV ions would produce a trail of only slightly-elongated point-like defects [18].

IV. Results

A. Microstructure

Low-resolution cross-sectional TEM micrographs of 100 MeV and 50 MeV irradiated samples are shown in Fig. 2. The large number of 10–50 nm particles visible in the sample are $(Y,Dy)_2O_3$ precipitates which act to improve isotropic flux pinning at 77 K [19]. Several horizontal extended defects are also visible, corresponding to *ab*-planar defects including Y124-type stacking faults [20]. Both the nanoparticles and planar defects are typically present in the pristine as-received samples. Following irradiation with 100 MeV Ag ions, extended ion damage tracks are visible as vertical linear features. These tracks are not continuous throughout the thickness of the film but instead form series of co-linear columns. Similar tracks have previously been observed for 74 MeV Ag ions [7].

In contrast, such extended tracks were not observed following irradiation with 50 MeV Ag ions. This is consistent with the expectation arising from the ion energy profile of Fig. 1 and Ref. [18] that damage tracks should consist of only slightly-elongated nanometer-sized particles for this incident energy.

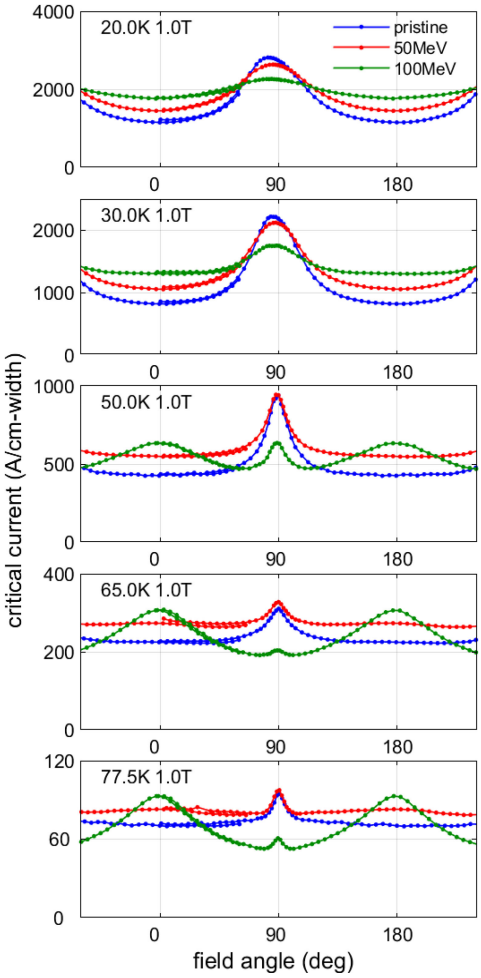

Fig. 3. Angular dependences of the critical current at 1 T applied field for temperatures ranging from 20 K to 77 K for a pristine (as-received) sample and samples irradiated with 50 MeV and 100 MeV Ag ions, both at a fluence of 2×10^{11} ions/cm^2.

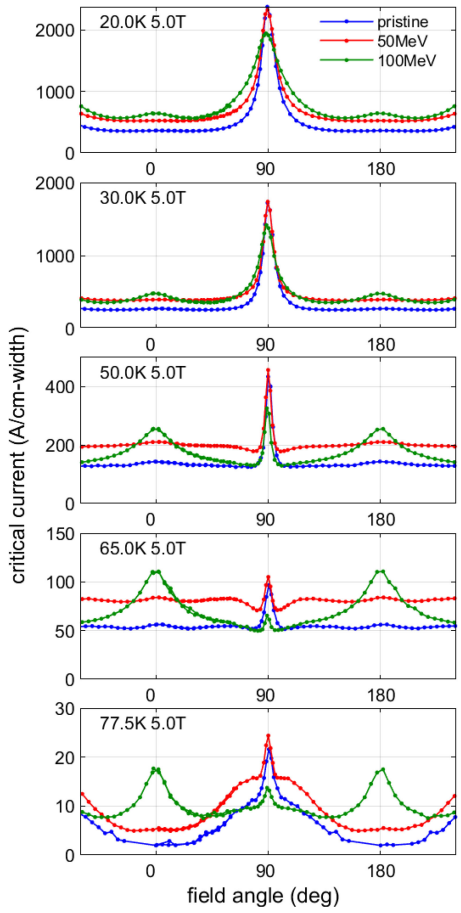

Fig. 4. Angular dependences of the critical current at 5 T applied field for temperatures ranging from 20 K to 77 K for a pristine (as-received) sample and samples irradiated with 50 MeV and 100 MeV Ag ions, both at a fluence of 2×10^{11} ions/cm^2.

B. In-Field Critical Current, Normal Incidence Irradiation

Flux pinning is most simply manifested in the DC critical current and critical-current anisotropy, which are functions of temperature T and magnetic field B. The temperature dependence reflects the variation of the superconducting coherence length which increases with increasing temperature suggesting that smaller pinning centers should be more effective at lower temperatures. The field dependence relates to the number density of pinning centers, which in the case of irradiation is linked mainly to the ion fluence, although different ion species or energies producing different sizes of defects may play into this as well. We show the critical current anisotropy for a pristine sample and samples irradiated at 50 MeV and 100 MeV, both at a fluence of 2×10^{11} ions/cm^2 corresponding to a matching field (at which each ion track pins one vortex) of $B_\phi = 4$ T. At this fluence, the superconducting transition temperature T_c was suppressed by less than 0.5 K. In Fig. 3 we show $I_c(\theta)$ for a range of temperatures from 20 K to 77 K, all at a relatively low field of 1 T, and in Fig. 4 we show the same for a moderate field of 5 T.

At 1 T and 77 K (Fig. 3) there is a clear qualitative difference between 50 MeV and 100 MeV irradiation. At 100 MeV a large and distinct peak appears in $I_c(\theta)$ at 0° (perpendicular magnetic field) corresponding to the irradiation direction. This reflects the presence of highly anisotropic pinning centers—the ion tracks—and has been well demonstrated with high-energy ion irradiation. This gives a significant enhancement of I_c for a limited range of angles near 0°, but then there is a reduction in I_c for a range of angles orthogonal to this direction. Taking the minimum value of I_c for each of these curves, $I_c^{\min}$, as a useful metric [21], there is a clear reduction in this quantity at 77 K, 1 T for 100 MeV irradiation. At 50 MeV on the other hand, the 0° peak is so broad as to be barely discernible and now I_c is enhanced, or at least not reduced, over the entire angular range relative to the pristine sample. In particular, $I_c^{\min}$ is improved by 12%.

As the temperature is reduced, the 0° peak for 100 MeV irradiation broadens, but also $I_c^{\min}$ improves relative to the pristine sample. Interestingly, by 30 K the $I_c(\theta)$ enhancement is almost isotropic and $I_c^{\min}$ is now significantly improved by 60%, becoming better even than the 50 MeV case (30%). $I_c(\theta)$ enhancement remains very nearly isotropic for 50 MeV over the full temperature range, consistent again with the expectation that this energy of irradiation introduces point-like defects.

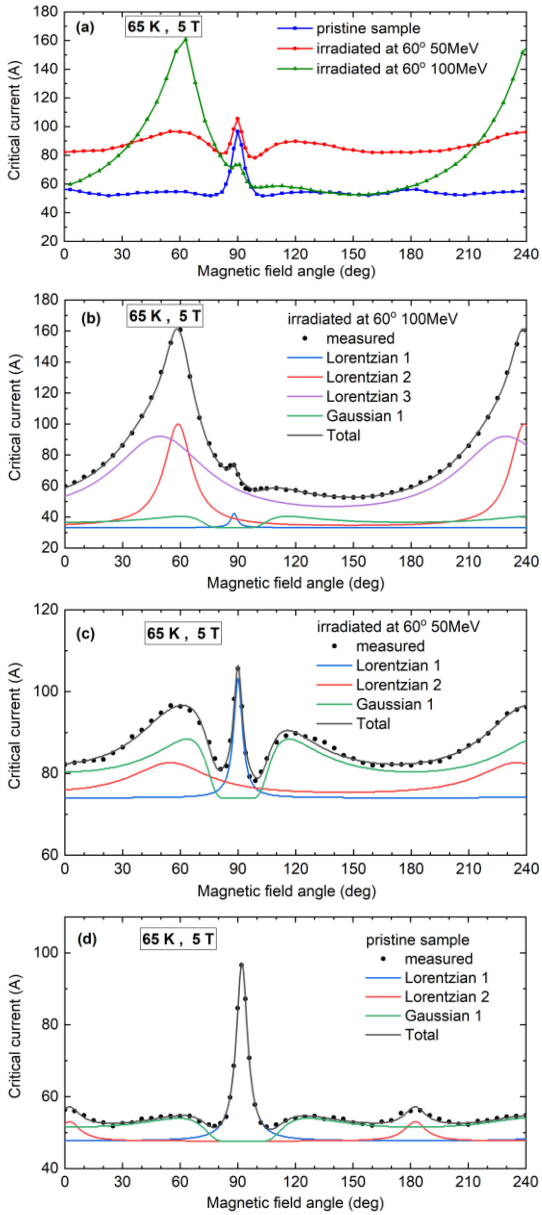

Fig. 5. (a) Comparison of critical current anisotropy at 65 K, 5 T of a pristine (as-received) sample, and samples irradiated with 50 MeV and 100 MeV Ag ions at a 60° inclination to the sample normal, and at a fluence of 2×10^{11} ions/cm^2. (b)-(d) Fits to each of the data sets using maximum entropy functional forms.

At 5 T (Fig. 4), 100 MeV irradiation now gives an improvement in I_c^{min} at 77 K, reflecting the greater importance of flux pinning at this field and especially the fact that we are increasing the irreversibility field for perpendicular field orientation. Again, 100 MeV irradiation produces peaks at 0° whereas 50 MeV irradiation produces a very flat $I_c(\theta)$ except near the *ab* plane, reflecting the columnar and point-like defects respectively. At 20 K both 50 MeV and 100 MeV irradiation produce nearly isotropic $I_c(\theta)$ enhancement. I_c^{min} of these commercial wires is enhanced at 20 K by 60% for 100 MeV and by 45% for 50 MeV irradiation. The field here is greater than the matching field, so it is likely that higher ion fluences are required to fully optimize the pinning enhancement.

C. Inclined Irradiation

To further examine the differences between 50 MeV and 100 MeV irradiation, we have irradiated samples with a 60° inclination relative to the normal, again with a fluence of 2×10^{11} ions/cm^2. $I_c(\theta)$ at 65 K, 5 T for each of these samples, compared to the pristine sample is shown in Fig. 5(a). A clear peak is observed at 60° for the 100 MeV case, but the peak is again barely discernible for 50 MeV. Further, at 50 MeV there is a similar but unexpected peak at 120°. This is explained by fitting the pinning profile in Fig. 5(b)–(d) using maximum entropy functions of the vortex path model [22]. For 100 MeV irradiation the 60° peak dominates the anisotropy (Fig. 5(b)). The peak is slightly asymmetric so requires two Lorentzian components to fit; the broad component centered at 50° may arise as an interaction between the multiple pinning populations present in the sample. The "extra" peak in the 50 MeV sample is explained in Fig. 5(c). There is a broad Lorentzian component at 60° corresponding to the irradiation angle, then there is also a very broad Gaussian component centered at 0° (and 180°). The Gaussian form bifurcates when very broad giving the appearance of two shoulders at intermediate angles. This enhances the peak at 60° and also produces the unexpected peak at 120°. We can see that this bifurcated Gaussian function is also present in the 100 MeV sample and even in the pristine sample (Fig. 5(d)); it represents a population of slightly anisotropic pinning centers with an overall *c*-axis alignment. The fit for 50 MeV shows that irradiation at this energy does produce slightly anisotropic pinning suggesting that the point-like defects are indeed slightly elongated along the irradiation direction.

V. Conclusion

We have performed Ag-ion irradiation of commercial REBCO wires at energies of 50 MeV and 100 MeV. Due to the silver cap layer the ion energy is calculated to be reduced to 32 MeV and 73 MeV respectively at the REBCO surface. By comparing TEM imaging and the critical current anisotropy over a range of temperatures and magnetic fields, we can identify a threshold incident energy of around 50 MeV above which the ion-damage tracks form columnar defects and below which they form point-like defects. At a fluence of 2×10^{11} ions/cm^2 (matching field 4 T), the critical current at the "worst angle", I_c^{min}, is enhanced by up to 59% for 100 MeV ions and by up to 46% for 50 MeV ions at 20 K. The ion fluence is not optimized and greater enhancements can be produced at higher fluence [23].

Acknowledgment

We acknowledge access to the Heavy-Ion Accelerator Facility funded under the National Collaborative Research Infrastructure Strategy (NCRIS), Australia.

References

[1] I. A. Sadovskyy *et al.*, "Toward superconducting critical current by design," *Adv. Mater.*, vol. 28, pp. 4593–4600, Mar. 2016.
[2] W.-K. Kwok, U. Welp, A. Glatz, A. E. Koshelev, K. J. Kihlstrom, and G. W. Crabtree, "Vortices in high-performance high-temperature superconductors," *Rep. Prog. Phys.*, vol. 79, Sep. 2016, Art. no. 116501.

[3] J. L. MacManus-Driscoll *et al.*, "Strongly enhanced current densities in superconducting coated conductors of $YBa_2Cu_3O_{7-x} + BaZrO_3$," *Nature Mater.*, vol. 3, pp. 439–443, May 2004.
[4] J. Gutiérrez *et al.*, "Strong isotropic flux pinning in solution-derived $YBa_2Cu_3O_{7-x}$ nanocomposite superconductor films," *Nature Mater.*, vol. 6, pp. 367–373, May 2007.
[5] N. M. Strickland *et al.*, "Enhanced flux pinning by $BaZrO_3$ nanoparticles in metalorganic deposited YBCO second-generation HTS wire," *Physica C*, vol. 468, no. 3, pp. 183–189, Feb. 2008.
[6] L. Civale *et al.*, "Vortex confinement by columnar defects in $YBa_2Cu_3O_7$ crystals: Enhanced pinning at high fields and temperatures," *Phys. Rev. Lett.*, vol. 67, no. 5, pp. 648–651, Jul. 1991.
[7] N. M. Strickland *et al.*, "Flux pinning by discontinuous columnar defects in 74 MeV Ag-irradiated $YBa_2Cu_3O_7$ coated conductors," *Physica C*, vol. 469, no. 23, pp. 2060–2067, Dec. 2009.
[8] N. M. Strickland, S. C. Wimbush, J. V. Kennedy, M. C. Ridgway, E. F. Talantsev, and N. J. Long, "Effective low-temperature flux pinning by Au ion irradiation in HTS coated conductors," *IEEE Trans. Appl. Supercond.*, vol. 25, no. 3, Jun. 2015, Art. no. 6600905.
[9] T. Sueyoshi *et al.*, "Flux pinning properties in YBCO films with growth-controlled nano-dots and heavy-ion irradiation defects," *Physica C*, vol. 530, pp. 72–75, 2016.
[10] T. Sueyoshi, "Modification of critical current density anisotropy in high-T_c superconductors by using heavy-ion irradiations," *Quantum Beam Sci.*, vol. 5, 2021, Art. no. 16.
[11] K. J. Kihlstrom *et al.*, "Large enhancement of the in-field critical current density of YBCO coated conductors due to composite pinning landscape," *Supercond. Sci. Technol.*, vol. 34, 2021, Art. no. 015011.
[12] D. X. Fischer, R. Prokopec, J. Emhofer, and M. Eisterer, "The effect of fast neutron irradiation on the superconducting properties of REBCO coated conductors with and without artificial pinning centers," *Supercond. Sci. Technol.*, vol. 31, Mar. 2018, Art. no. 044006.
[13] M. Leroux *et al.*, "Rapid doubling of the critical current of $YBa_2Cu_3O_{7-\delta}$ coated conductors for viable high-speed industrial processing," *Appl. Phys. Lett.*, vol. 107, 2015, Art. no. 192601.
[14] M. W. Rupich *et al.*, "Engineered pinning landscapes for enhanced 2G coil wire," *IEEE Trans. Appl. Supercond.*, vol. 26, no. 3, Apr. 2016, Art. no. 6601904.
[15] M. W. Rupich *et al.*, "Second generation wire development at AMSC," *IEEE Trans. Appl. Supercond.*, vol. 23, no. 3, Jun. 2013, Art. no. 6601205.
[16] N. M. Strickland *et al.*, "Extended-performance supercurrent cryogen-free transport critical-current measurement system," *IEEE Trans. Appl. Supercond.*, vol. 31, no. 5, 2021, Art. no. 9000305.
[17] J. F. Ziegler, M. D. Ziegler, and J. P. Biersack, "SRIM – the stopping and range of ions in matter," *Nucl. Instrum. Meth. B*, vol. 268, pp. 1818–1823, Jun. 2010.
[18] M. Toulemonde, S. Bouffard, and F. Studer, "Swift heavy ions in insulating and conducting oxides: Tracks and physical properties," *Nucl. Instrum. Meth. B*, vol. 91, pp. 108–123, 1994.
[19] J. A. Xia *et al.*, "TEM observation of the microstructure of metal organic deposited YBCO with dy additions," *Supercond. Sci. Technol.*, vol. 20, pp. 880–885, 2007.
[20] E. F. Talantsev, N. M. Strickland, S. C. Wimbush, J. G. Storey, J. L. Tallon, and N. J. Long, "Hole doping dependence of critical current density in $YBa_2Cu_3o_{7-\delta}$ conductors," *Appl. Phys. Lett.*, vol. 104, 2014, Art. no. 242601.
[21] N. M. Strickland and S. C. Wimbush, "The magnetic-field dependence of critical current: What we really need to know," *IEEE Trans. Appl. Supercond.*, vol. 27, no. 4, Jun. 2017, Art. no. 8000505.
[22] N. J. Long *et al.*, "Relating critical currents to defect populations in superconductors," *IEEE Trans. Appl. Supercond.*, vol. 23, no. 3, Jun. 2013, Art. no. 8001705.
[23] A. A. Soman *et al.*, "The role of stacking faults in the enhancement of the *a-b* plane peak in silver ion-irradiated commercial MOD RE-BCO wires," *IEEE Trans. Appl. Supercond.*, vol. 32, no. 4, Jun. 2022, Art. no. 8000405.